Earth Systems and Environment (2019) 3:551–562
https://doi.org/10.1007/s41748-019-00122-z

ORIGINAL ARTICLE

Analysis of Absorption Characteristics and Source Apportionment of Carbonaceous Aerosol in Arid Region of Western India

M. Sateesh[1,3] · V. K. Soni[2] · P. V. S. Raju[1] · V. S. Prasad[3]

Received: 24 June 2019 / Accepted: 18 September 2019 / Published online: 27 September 2019

Abstract

The present work analyses the equivalent Black Carbon (EBC) data obtained using Aethalometer (AE-33) located at India Meteorological Department, Jodhpur, Rajasthan during the year 2016. The annual mean EBC concentration is 5.76 μg m^{-3} and the monthly mean concentration is maximum (12.12 μg m^{-3}) in January and minimum (1.27 μg m^{-3}) in December. The seasonal mean of wind speeds are 1.94, 2.02, 1.34, 1.02 m s^{-1} and the calm percentages are 7, 5.7, 28.7, 25.7% during pre-monsoon (MAM), monsoon (JJAS), post-monsoon (ON) and winter (DJF), respectively. The night time EBC concentrations are more than the day time concentrations due to the shallowness of the boundary layer and local anthropogenic activities. The Concentrated Weighted Trajectories (CWT) are calculated using back trajectories ending at 100 m above ground level at Jodhpur station using National Centre for Medium Range Weather Forecast (NCMRWF) Global Forecast System (GFS) based reanalysis T574 data. The CWT, directional source region analysis reveals the effect of long-range transport in the winter season with a 60% of probability of source regions from the W, NW direction of observational site. Source apportionment also carried out by assuming alpha (at 470-, 950-nm wavelengths) close to 1 for anthropogenic emissions and alpha close to 2 for biomass burning aerosols. The monthly mean biomass burning concentration is found maximum (2.58 μg m^{-3}) in November and minimum (0.22 μg m^{-3}) in July.

Keywords Equivalent black carbon · Seasonal variation · Angstrom exponent · Ventilation coefficient · Concentrated weighted trajectories

1 Introduction

Carbonaceous aerosols in the atmosphere are due to the combustion of fossil fuel, biomass (Ensor et al. 1971; Prather et al. 2008). Light absorbing carbonaceous (LAC) aerosols are mainly composed of black carbon and organic carbon which significantly affect the incoming solar radiation (Moosmüller et al. 2009). The increasing demand of various sectors causes the emission of carbonaceous aerosols in the form of incomplete combustion of carbon containing fossil fuel, biomass and bio fuel (Babu et al. 2013). Carbonaceous aerosols have similar sources as that of fine particulate matter with larger emissions arising from burning of residential bio-fuel, agricultural residue and industrial coal (Eck et al. 2010). The LAC aerosols play a major role in the climatic effects due to its large radiative forcing in the atmosphere (IPCC 2014). The black carbon aerosol measured using optical absorption methods are known as Equivalent Black Carbon (EBC; Petzold et al. 2013). EBC aerosols absorb incoming solar radiation and re-radiate in the form of infrared radiation and thereby causing warming of atmosphere surrounding them (Henriksson et al. 2014; Lack and Cappa 2010; Stier et al. 2007). EBC aerosols are short-lived climate forcing agent and secondary important contributor to global warming after greenhouse gas carbon dioxide (Bond et al. 2013). Because of shorter lifetime compared to greenhouse gases, EBC aerosols have become subject of research for investigating their role on climate and appropriate mitigation strategies. The aerosol characteristics and abundance can increase or decrease the cloud cover (Kaufman and Koren,

✉ P. V. S. Raju
pemmani@gmail.com; pvsraju@jpr.amity.edu

1 Centre for Ocean-Atmospheric Science and Technology (COAST), Amity University Rajasthan, Kant Kalwar, Jaipur, Rajasthan, India

2 Environmental Monitoring and Research Center, India Meteorological Department, Lodhi Road, New Delhi, India

3 National Centre for Medium Range Weather Forecasting, Noida, UP, India

2006) Black carbon and mineral dust (primarily hematite and various clays) are major light absorbing components of the aerosols in the atmosphere (Ramanathan et al. 2007; Otto et al. 2009; Moosmüller et al. 2009). However, spectral dependence of absorption of both the components is significantly different. Black carbon aerosols absorb light in entire visible spectrum (Bond et al. 2006) but mineral dust shows stronger absorption towards shorter wavelengths in blue and green spectrum (Sokolik and Toon, 1996). Tegen et al. (1997) estimated that absorbing aerosols contribute between 24 and 53% to the global total aerosol optical depth. The specific absorption coefficient of dust is much lower compared to black carbon aerosol but higher atmospheric abundance of dust over a region can cause a substantial absorption of solar radiation. The larger mineral dust aerosol generally found in the lowermost atmosphere while lighter absorbing anthropogenic aerosol can dwell over the land and extend vertically in the atmosphere to greater heights.

The significant and persistent dust sources are located in "global dust belt" which extends from the west-coast of North Africa, over Middle East, Central and South Asia and covers the deserts of Sahara, Arabian Peninsula, Gobi and Taklimakan (Prospero et al. 2002). The deserts in West Asia are considered to be large source of mineral dust aerosol in the atmosphere. The dust raising convective activities and strong winds can uplift mineral dust aerosols into the atmosphere (d'Almeida 1986; Goudie and Middleton 2001; Engelstaedter et al. 2006). These dust aerosols can be transported to long distances away from the source regions over large distances at the continental and intercontinental scales and play an important role in atmospheric radiative balance at surface and top of the atmosphere. The Thar Desert is one of the largest sources of dust over Northern India. The long-range transport of dust from Arabian Peninsula also affects the west and north India. The higher atmospheric aerosol concentrations lead to the visibility degradation (Bäumer et al. 2008; Singh and Dey 2012) as well as dimming of solar radiation (Soni et al. 2016; Yu 2002). The uncertainties in atmospheric burden of aerosols introduce strong uncertainty in the estimation of radiative forcing (Haywood and Ramaswamy 1998) The EBC aerosol concentration exhibits strong seasonal variation. The seasonal variation can be attributed to variation in meteorological conditions, chemistry and physical loss processes, emission sources and their strength in different seasons. The widespread agriculture waste burning takes place in northern and north-western part of India during October and November. The bio-fuel combustion for domestic heating and cooking also varies seasonally. The dust raising convective activities are more common during summer in northern India. Further, the meteorology plays an important role in seasonal variation of aerosol concentration.

EBC aerosol studies from arid region are very sparse. This is the first study on EBC from Jodhpur located in the Thar Desert region. Temporal characteristics of absorption coefficient, EBC and BB concentrations have been discussed in detail. Furthermore, the relationship between EBC and meteorological conditions is used to investigate the impact on local EBC variations. The site-specific compensation factors (Virkkula et al. 2015) which are dependent on humidity and type of aerosols have been used for the aged aerosols. Finally, back trajectories analysis was used to investigate the source–receptor relationships and the timescales of regional transport and its effect on the observed EBC and BB concentration. The detail description of the analysis site and general meteorological features and data are given in Sects. 2 and 3. The results and discussion are given in Sect. 4. The main findings the results are summarized in Sect. 5.

2 Site Description and Meteorological Condition

The Thar Desert, also known as the Great Indian Desert, is a large land-locked hot and arid region in the north-western part of the Indian subcontinent. The Thar Desert is the easternmost extension of the vast Saharo-Arabian deserts (Singhvi and Kar, 2004). Major portion of the Thar Desert lies in Rajasthan state of India. Jodhpur (23.30°N, 73.01°E, 231 m amsl) which is part of the Thar Desert receives 270-mm rainfall during monsoon season, while annual rainfall is of the order of 298 mm. Jodhpur is the largest city in the region, lies in the scrub forest zone and has undulating terrain. The normal annual rainy days over Jodhpur districts are 59 days. Jodhpur is characterized by extreme weather conditions like low and highly variable rainfall, high ambient temperatures, strong winds and low humidity. The arid condition in Jodhpur leads to frequent dust raising convective activities in during summer months. Higher concentration of dust aerosols is observed during summer compared to other seasons. In this study, the Automatic Weather Station data were used to analyze the meteorological condition over the observational site. The daily mean variation of temperature, pressure and relative humidity are depicted in Fig. 1. The Meteorological condition of atmospheric temperature indicated warming during prior to the monsoon rains and cooling during winter season. The atmospheric pressure (Fig. 1b) shows the lowest in the monsoon season and high pressure during the winter period. The relative humidity indicates that higher values are noticed during the rainy season, whereas lower values observed during pre-monsoon season. These higher humidity levels extended up to September also due to the delay in retreat of the monsoon. The monthly wind rose plots with frequency count, clam condition percentage and the mean wind speed was illustrated in Fig. 2. The maximum mean wind is recorded during May (2.27 ms^{-1}) and minimum in November (0.88 ms^{-1})

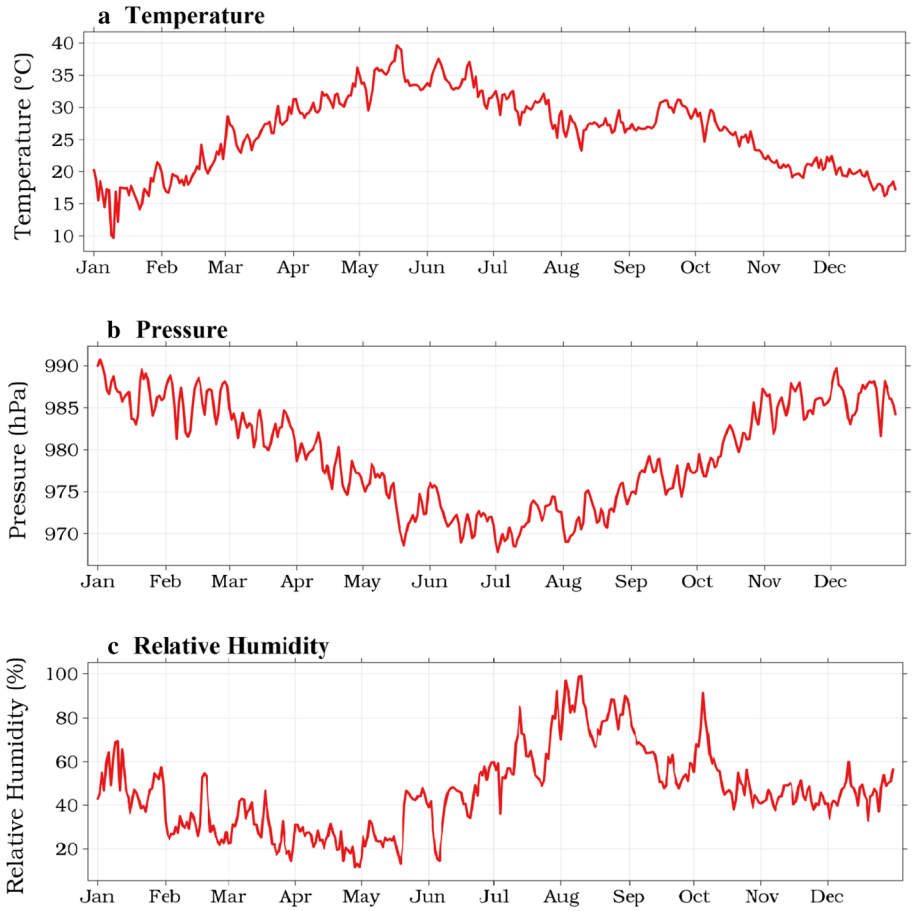

Fig. 1 Time series of daily averaged meteorological variables during 2016 for **a** air temperature, **b** atmospheric pressure and c) humidity

with calm condition percentage (49.2%). The maximum wind during May and June is source of dust/sand storm over this region. The annual mean meteorological variables of temperature, pressure, relative humidity and wind speed (Table 1) over the Jodhpur station observed are 26.7 °C, 979 hPa, 46.4% and 1.38 ms^{-1} respectively. The maximum (minimum) temperature observed during May (January) is 40 °C (7 °C). In general pre-monsoon month of May and monsoon season, the maximum rainfall occurs which corroborates with lowest atmospheric pressure and increase of relative humidity over this region (Fig. 1b, c).

3 Data

The Equivalent Black Carbon (EBC) aerosol concentration is measured at Jodhpur using seven wavelengths Aethalometer, model AE-33 (MAGEE Scientific, USA) for the year 2016. Aethalometer measures aerosol absorption at seven discrete wavelengths (370, 470, 520, 590, 660, 880 and 950 nm) with a temporal resolution of 1 min. The PM2.5 sampling inlet connected with the Aethalometer is mounted at about 10-m height above the ground. The basic measured parameter by Aethalometer is the spectral aerosol absorption coefficients determined by incremental attenuation of the incident light transmitted through the sample spot on a quartz fiber filter. The model AE-33 employs dual-spot technique to eliminate 'aerosol loading' effect using real-time compensation algorithm based on simultaneous measurements of two attenuation coefficients with different flow rates (Drinovec et al. 2015). More details of Aethalometer AE-33 and accuracy of measurement can be found in Drinovec et al. (2015). The measurement of absorption coefficient at 880 nm with mass absorption cross Sect. 7.77 $m^2\ g^{-1}$ is used to determine EBC concentration. The biomass burning component of EBC aerosol is estimated using Sandradewi model (Sandradewi et al. 2008a). The BB % is calculated as a ratio of BB concentration to the EBC concentration. Ventilation rate/coefficient, a product of planetary boundary layer height (m) and surface wind speeds (m s^{-1} at 10 m height) (Ghiaus et al. 2006; Chan et al. 2012), is obtained from NCMRWF reanalysis data. Here onwards, ventilation rate/coefficient is represented as ventilation coefficient (VC). The details of T574 reanalysis data and its description can be found in Prasad et al. (2017). The meteorological data (wind, relative humidity and atmospheric pressure) were obtained from meteorological station of India Meteorological Department, Jodhpur. A 5-day back trajectory analysis also carried out

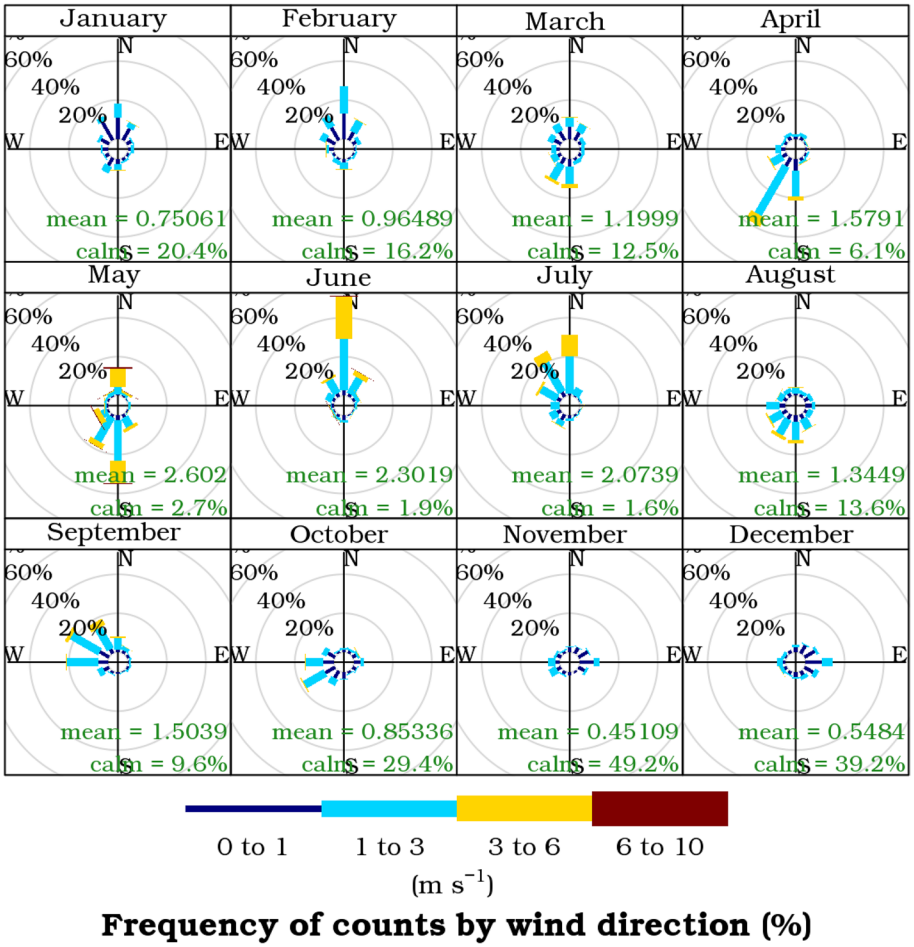

Fig. 2 Monthly wind rose plots at Jodhpur station during 2016 (frequency count by wind direction given in %)

Table 1 Monthly and seasonal averaged temperature (°C), pressure (hPa), Humidity (%), Wind Speed (m s^{-1}), eBC (ngm^{-3}), AE470950, BB(μg m^{-3}), BB (%) and Ventilation Coefficient (m^2 s^{-1}) Values in the bracket denote the % of biomass burning in eBC

S. no.	Months	Temp (°C)	Pressure (hPa)	Humidity (%)	Wind Speed	eBC	AE470-950	BB	VC
1	January	17.2	986.7	48	0.74	12,121	1.2402	2331(18.3)	554
2	February	19.8	985.9	32	0.97	5738	1.2640	1137 (20.4)	827
3	March	26.4	982.6	29	1.20	3694	1.2369	767(19.1)	1579
4	April	30.9	978.4	23	1.57	3558	1.2168	601 (17.4)	2245
5	May	34.7	974.1	30	2.60	2492	1.2765	541 (22.6)	3813
6	June	34.0	972.2	42	2.30	1658	1.2102	289 (17.5)	2786
7	July	30.2	971.4	63	2.07	1416	1.1917	221 (16.2)	1915
8	August	27.2	972.4	82	1.36	1964	1.1744	274 (14.1)	756
9	September	28.7	976.8	61	1.51	2976	1.2078	472 (16.2)	1440
10	October	26.3	980.7	55	0.86	5911	1.1779	831 (13.8)	1011
11	November	20.9	985.5	44	0.45	13,127	1.2782	2583 (21.6)	409
12	December	19.0	986.3	46	0.55	12,711	1.2651	2481 (20.3)	391
13	Spring (MAM)	30.8	978.3	28	1.81	3247	1.2436	637 (19.7)	2571
14	Summer (JJAS)	30.0	973.2	62	1.81	2003	1.1960	314 (16.0)	1724
15	Autumn (ON)	23.6	983.1	49.5	0.65	9519	1.2280	1709 (17.7)	710
16	Winter (DJF)	18.8	986.2	41	0.75	10,282	1.2563	2000 (19.6)	594

for every hour at observatory location at a reception height of 100 m using the NCMRWF reanalysis data with a spatial resolution of 25 km during the study period.

4 Results and Discussion

4.1 Spectral Variation of Aerosol Absorption Coefficient

The absorption characteristics are determined by physical and chemical properties of aerosol. The spectral dependence of aerosol absorption coefficient is of importance to study the radiative effects of aerosols as well as source apportionment of carbonaceous aerosol (Sandradewi et al. 2008a, b). The monthly mean absorption spectrum at the observational site is shown in Fig. 3. The aerosol absorption coefficient (M m^{-1}) decreases monotonically with increase in wavelength during all the months. The aerosol absorption was stronger in November, December and January at all seven wavelengths. The highest absorption is observed in January during which lowest ambient air temperature and very shallow boundary layer occurs. The crop residue burning is frequent during post-monsoon season and peaks in November month in the North-Western parts of India. The long-range transport also influences the temporal variation in the winter months. The lowest absorption coefficient is observed during the monsoon months. The local influence during the monsoon season (JJAS) is minimum as air mass trajectories are mainly from Arabian Sea.

4.2 Temporal Variations

The spectral dependence of absorption coefficient can be defined by the power law and parameterized by $b_{abs}(\lambda) \sim \lambda^{-\alpha}$. Aerosol absorption Angström exponent (α) was derived to characterize the spectral dependence of absorption coefficient (b_{abs}). The Alpha values were calculated using the following Eq. 1

$$\frac{b_{abs}(\lambda_1)}{b_{abs}(\lambda_2)} = \left(\frac{\lambda_1}{\lambda_2}\right)^{-\alpha}, \tag{1}$$

$$BC_{BB} = \frac{\left(\frac{b_{abs}(\lambda_1) - b_{abs}(\lambda_2) \times \left(\frac{\lambda_1}{\lambda_2}\right)^{-\alpha FF}}{\left(\frac{\lambda_1}{\lambda_2}\right)^{-\alpha BB} - \left(\frac{\lambda_1}{\lambda_2}\right)^{-\alpha FF}}\right)}{b_{abs}(\lambda_2)} \times eBC, \tag{2}$$

Or

$$BC_{BB} = eBC\left[\frac{\alpha - b}{a - b}\right], \tag{3}$$

where the wavelengths λ_1 and λ_2 are 470 and 950 nm. The a, b are consideration of α for biomass ($a = 2$) and fossil fuel ($b = 1$).

Some measurement studies found that $\alpha \sim 1$ for aerosols < 50 nm diameter where externally mixed black carbon dominates absorption (Moosmüller et al. 2009, 2011). However, the AAE for ambient aerosols (measured between a short and long visible wavelength) has often been observed

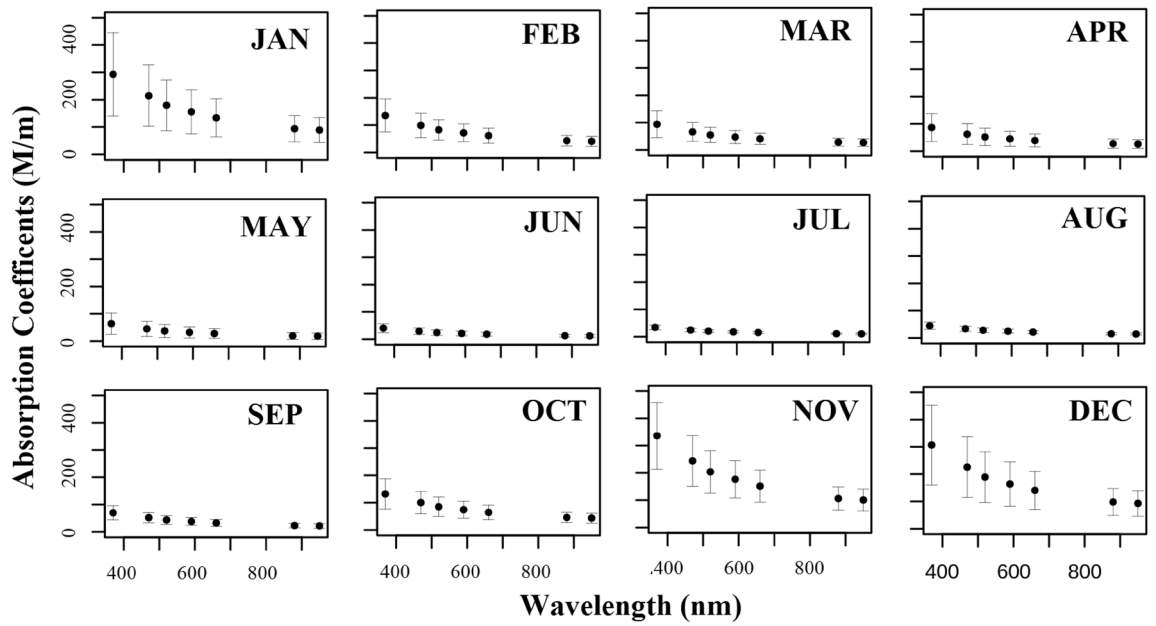

Fig. 3 Monthly mean mass absorption spectrum with standard deviation for Jodhpur station during 2016

to be larger than 1. Numerous factors contribute to these observations including absorption by BC which internally mixed with non-absorbing material, and absorption by non-BC absorbers of brown carbon (BrC) or desert dust (Russell et al. 2010; Kirchstetter et al. 2004). The source apportionment of biomass burning and traffic emissions is calculated using Eq. 2. For simplicity, the Eq. 2 can be written as Eq. 3. The daily mean temporal variation of EBC by levels of Alpha, and Alpha by levels of BB is shown in Fig. 4. The temporal variation of EBC is following the seasonal patterns along with the inverse relation to the planetary boundary layer.

Figure 4a presents variation of EBC by levels of Alpha in winter months. The Alpha values reach to a maximum value of 1.5 in November month due to the influence of crop residue burning smoke around the Jodhpur region. The higher Alpha value is also reported in the end of April month during which also crop residue biomass burning is reported in the region. The Alpha value ~ 2 indicates the presence of biomass burning aerosols, whereas ~ 1 represents traffic emissions (Drinovec et al. 2013; Sandradewi et al. 2008b; Zotter et al. 2017), Alpha value ~ 1.2 shows the existence of mixed type of aerosols from traffic emissions and local anthropogenic activities. Alpha values ~ 1.5 shows the existence of biomass burning aerosols. Still, there is a large uncertainty in the site-specific alpha value in the fixing of source apportionment of BC and BB (Healy et al. 2017; Zotter et al. 2017). The increase of BB aerosol concentration in November is due to the transport of pollutants from nearby region. The stable atmospheric conditions during November help in accumulation of pollutants as the highest frequency of calm wind condition of 49.2% is observed during this month (Fig. 2). As seen in Fig. 4b, the higher BB concentrations are also found in the December and January months due to the local anthropogenic activities and increased biomass burning for domestic heating. During this period, the Alpha values also increase (> 1.2) which depict high concentrations of fine mode particles.

The meteorology together with the emissions plays key role in determining the concentration of pollutant at any location. The monthly mean and seasonal mean values of meteorological variable (temperature, pressure, relative humidity and wind speed) along with the observed EBC, Alpha, BB and BB % are shown in Table 1. The monthly mean higher temperatures are observed in summer months May and June; higher atmospheric pressure in winter months November, December, January and February months; relative humidity in July, August, and September; and higher wind speed in May, June and July months. The higher EBC and BB concentrations are observed in the winter months. The annual EBC, BB, Alpha (AE470_950) and BB % are 5.76 μg m^{-3}, 1.07 μg m^{-3}, 1.23 and 18% respectively.

4.3 Diurnal Variation

The diurnal variation of EBC concentration, BB concentration and ventilation coefficient are depicted in Fig. 5. The observed EBC concentration (Fig. 5a) showed strong diurnal variability caused by local weather conditions and emission characteristics. The VC is high in the daylight time as compared to the night time and also shows seasonal variation. The ventilation coefficient is very high in the summer months and low in the winter night time. The annual mean ventilation coefficient is 1595 m^2 s^{-1}. The monthly mean diurnal variation is small during the monsoon season. Observed EBC concentrations are significantly higher

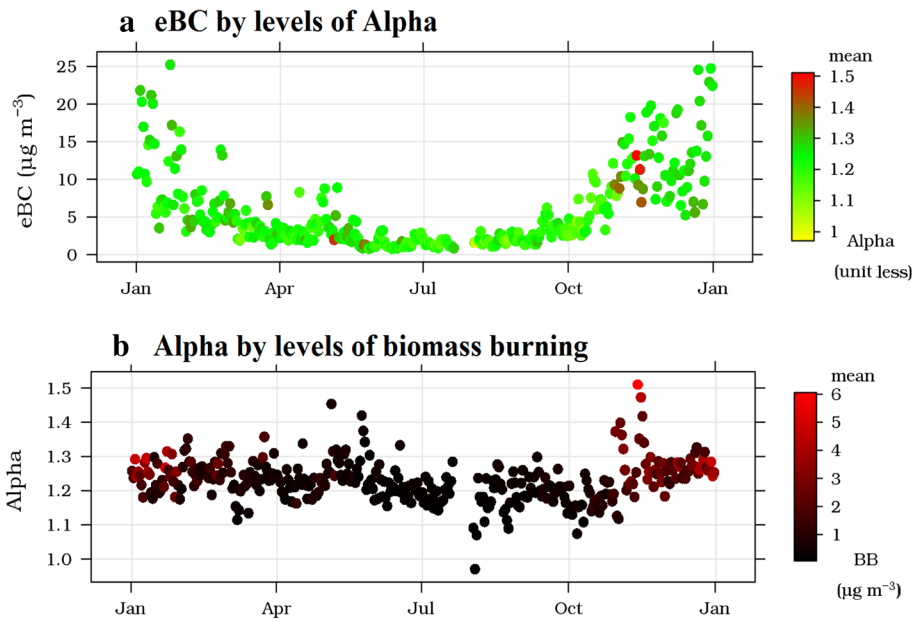

Fig. 4 Temporal variation of **a** equivalent black carbon (μg m^{-3}) by levels of Alpha. **b** Alpha (unit less) by levels of biomass burning (μg m^{-3}) at Jodhpur station

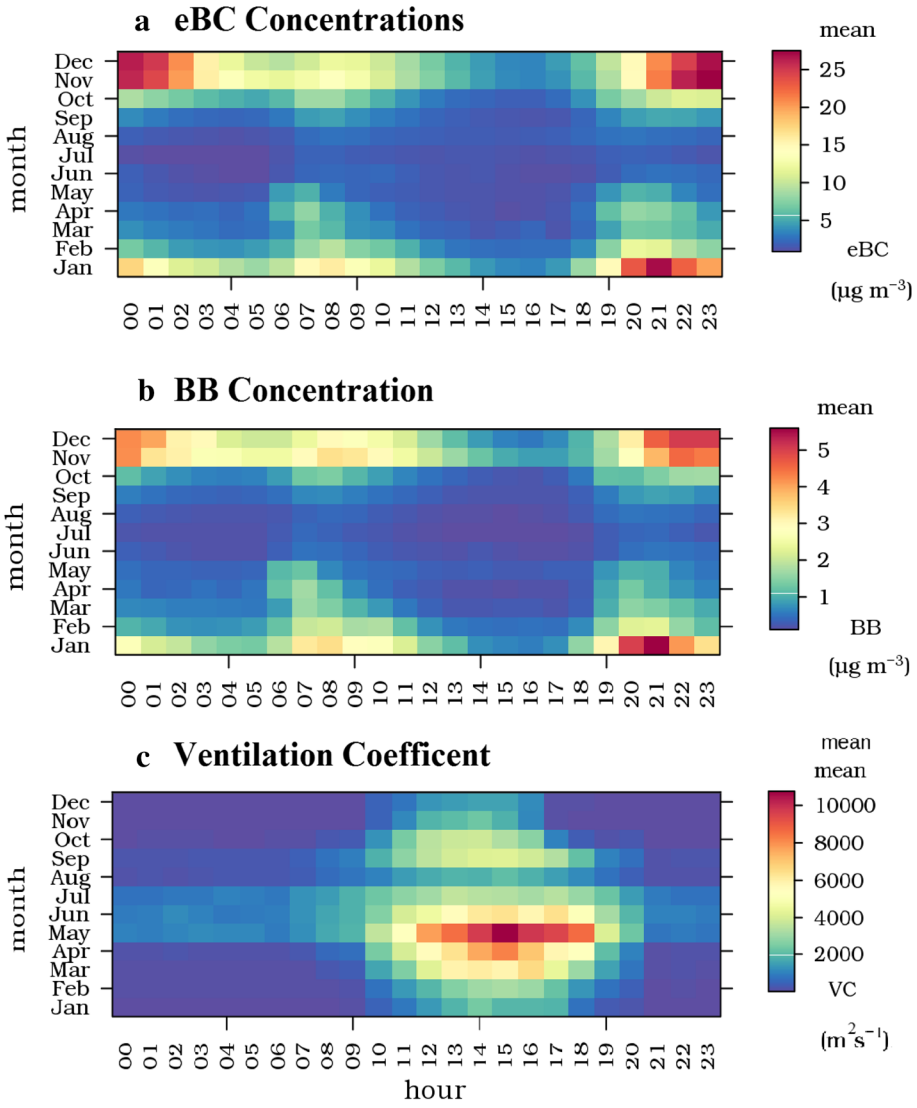

Fig. 5 Diurnal variation of **a** eBC concentrations in µg m^{-3} (IST time zone), **b** BB concentrations in µg m^{-3} (IST time zone) and **c** ventilation coefficient in m^2 s^{-1}

in the night as compared to the noon during winter. The increase in EBC and BB concentrations in the night during winter season is due to the local anthropogenic activities such as enhanced domestic heating from biomass and biofuel burning.

4.4 Potential Source Identification using Bivariate Analysis

The bivariate polar plots (Henry et al. 2002; Carslaw and Beevers 2013; Grange et al. 2016) of EBC and BB concentration as a function of wind speed and wind direction show dispersion with higher wind speeds. The distribution of bivariate plot for Equivalent Black Carbon (EBC) concentration and Bio-mass Burning (BB) concentration is depicted in Fig. 6 and 7. The high EBC and BB concentration in January month is due to the small magnitude of wind speeds. The January monthly mean of wind speed is 0.94 m s^{-1} and ventilation coefficient is 554 m^2 s^{-1}. The EBC concentrations were generally lower than the annual mean with winds coming from the North, South, and South-East directions. This kind of EBC and wind direction pattern is found from March to September. During winter, local emissions significantly affect the EBC concentration, most likely due to the domestic heating activity. Similar pattern for BB and wind direction was observed. The highest EBC and BB concentrations were mostly associated with the lower winds (< 2 m/s), whereas the concentrations decreased as the wind speed increases in all the sectors. This suggests that local emissions are dominant in determining the concentration of EBC and BB.

The aerosol loading compensation parameter K is determined in real time for each wavelength of Aethalometer AE33. The parameter K can also be used as a proxy to identify the source of Black Carbon aerosols (Drinovec et al. 2015, 2017; Virkkula et al. 2015). The higher value

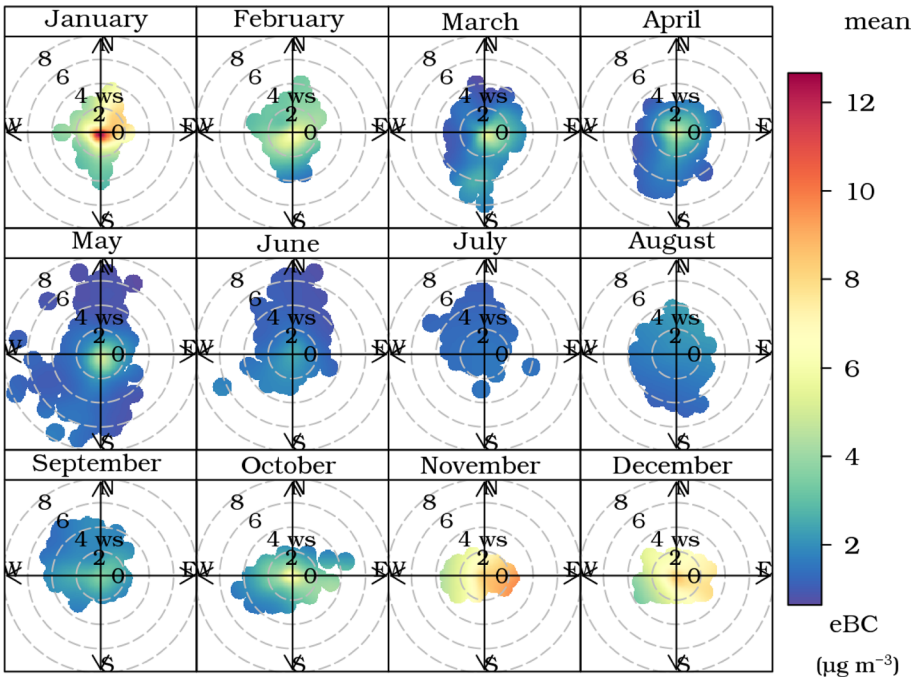

Fig. 6 Bivariate plot for equivalent black carbon (eBC) concentrations in μg m^{-3}

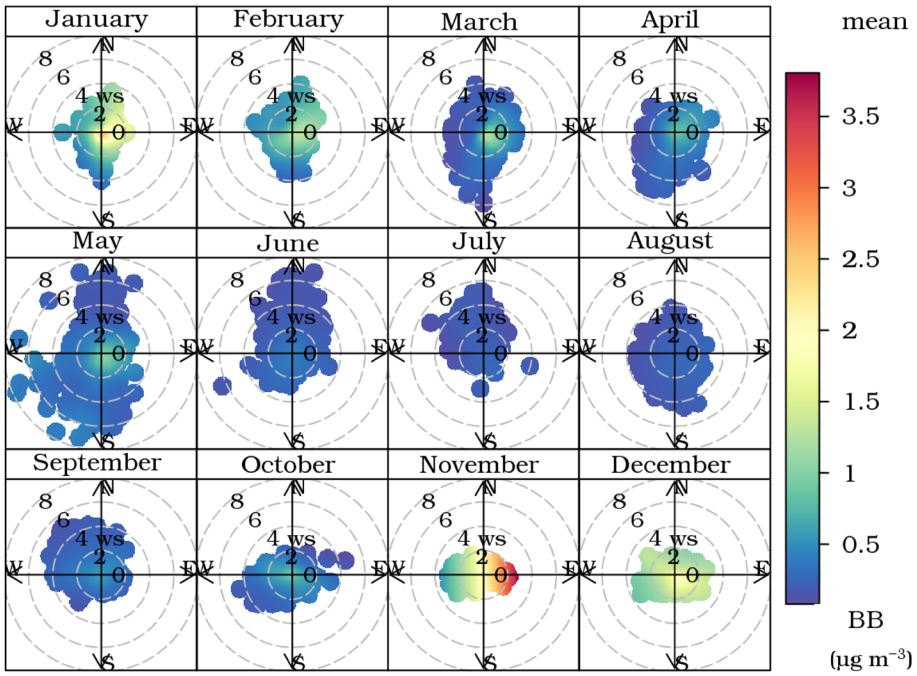

Fig. 7 Bivariate plot for Biomass Burning (BB) concentrations (μg m^{-3})

of compensation parameter, K, is an indicator for the local and freshly emitted black carbon aerosols; whereas the lower value of K indicates the aging and coating during long-range transport (Virkkula et al. 2015; Drinovec et al. 2015, 2017). The K values are reaching a maximum of 0.01 during postmonsoon and winter season at Jodhpur station (Fig. 8) with strong absorption in the lower wavelength spectrum (Fig. 3). It may be due to the extreme crop residue burning and Diwali festival (Sateesh et al. 2018) over north India in the month of November (Sateesh et al. 2018). Local aerosols with lower K values (< 0.003) are reported at the observational station during May and June–September months.

4.5 Monthly Back Trajectory Analysis

Intra-seasonal variation in aerosol mass concentration is mostly location specific of the station and can easily be analyzed by air mass back trajectories. To study the transport

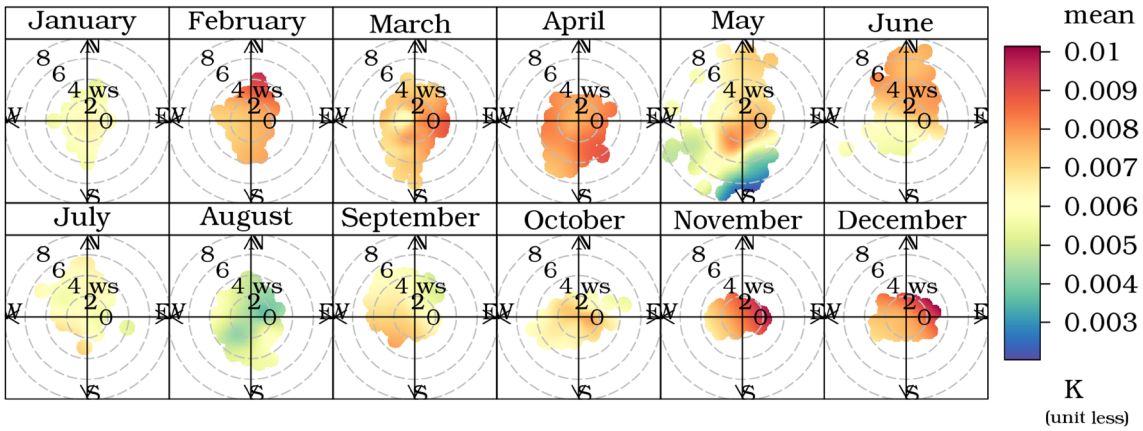

Fig. 8 Monthly Concentrated Weighted Trajectories of eBC concentrations in μg m^{-3} over Jodhpur station during 2016

pathways and potential aerosol source regions, we carried out backward trajectory analysis. Back trajectories were estimated with the Hybrid Single-Particle Lagrangian Integrated Trajectories (HYSPLIT) model (Draxler, 1998; Stein et al. 2015) using 0.25° × 0.25° horizontal resolution meteorological data from the National Centre for Medium Range Weather Forecasting (NCMRWF) by considering the surface variables like 10-m wind velocities, surface pressure, 2-m height temperature, specific humidity, topography and 1000, 950, 925,850, 700, 600, 500, 400, 300, 250, 200, 150, 100 level of winds, potential height, relative humidity, specific humidity, temperatures. Five-day back trajectories were calculated every hour ending at 100 m above the ground level. Air mass backward trajectory cluster analysis and Concentration Weighted Trajectory (CWT) analysis were carried out to examine the association between trajectories and EBC/BB concentration in ambient air arriving at Jodhpur and illustrated in Fig. 9.

The concentration weighted trajectories help in examining the contribution from local and regional sources (Fleming et al. 2012). From the CWT model analysis, major sources of EBC and BB influencing Jodhpur are primarily localized in regional areas. The North-west region comprising Pakistan, Punjab and Haryana can be considered as potential emission source regions during winter months. The inflow of air masses traveling over these regions is accountable for the

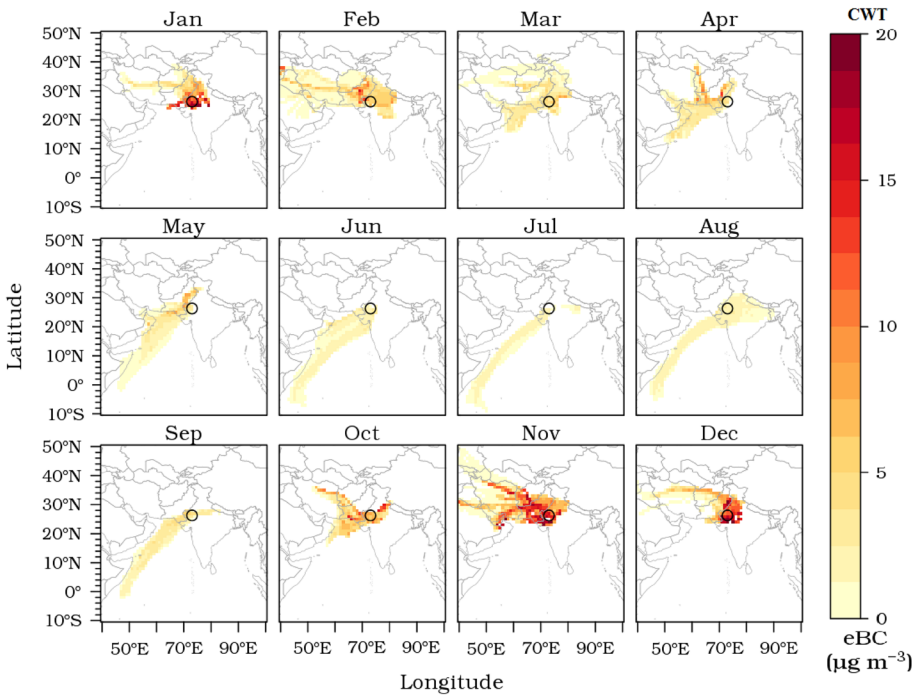

Fig. 9 **a** Cluster groups C1, C2, C3 and C4 at Jodhpur, 2016. **b** eBC concentrations of four groups of clusters. **c** BB concentrations of four group of clusters. (Time in UTC)

transport of EBC and BB aerosols to the receptor site Jodhpur which is added on top of the locally emitted. There are long-range trajectories present in various directions based on the seasons. Arabian Sea air masses are coming to the observational site starting from the May to September months in which the EBC concentrations are very low. The trajectories during post-monsoon season are observed due to the result in high EBC concentrations (Fig. 9). The December month trajectories are mostly coming from Eastern side of the observational site which results in high EBC concentrations.

4.6 Cluster Analysis

An error on the order of 20% of the distance traveled has been reported for trajectories of duration longer than 24 h (Stohl 1996,1998). The statistical analysis of a large number of trajectories arriving at a location over a longer duration reduces the error of trajectory analysis. In view of this, the cluster analysis of back trajectories is an appropriate method to categorize the air masses reaching at a specific site. Cluster analysis is a multivariate statistical technique that groups large number of trajectories into a smaller number of clusters of similar trajectories (Fleming et al. 2012). Five-day back trajectories reaching the station at 100 m above ground level were categorized into four dominant clusters (C1, C2, C3 and C4) based on the Euclidian distance approach (Ashbaugh et al. 1985; Sirois and Bottenheim 1995; Carslaw 2015; Carslaw and Ropkins 2012). The most abundant cluster C1 contains 40.8% of trajectories mainly coming from the North-west direction (Fig. 10a). The cluster C2 represents 26.8% of trajectories arriving from Western side of the observational site. The C3, C4 clusters are coming from the Arabian Sea with 17.5%, 14.9% trajectories, respectively. The cluster means of EBC and BB in μg m^{-3} are shown in Table 2.

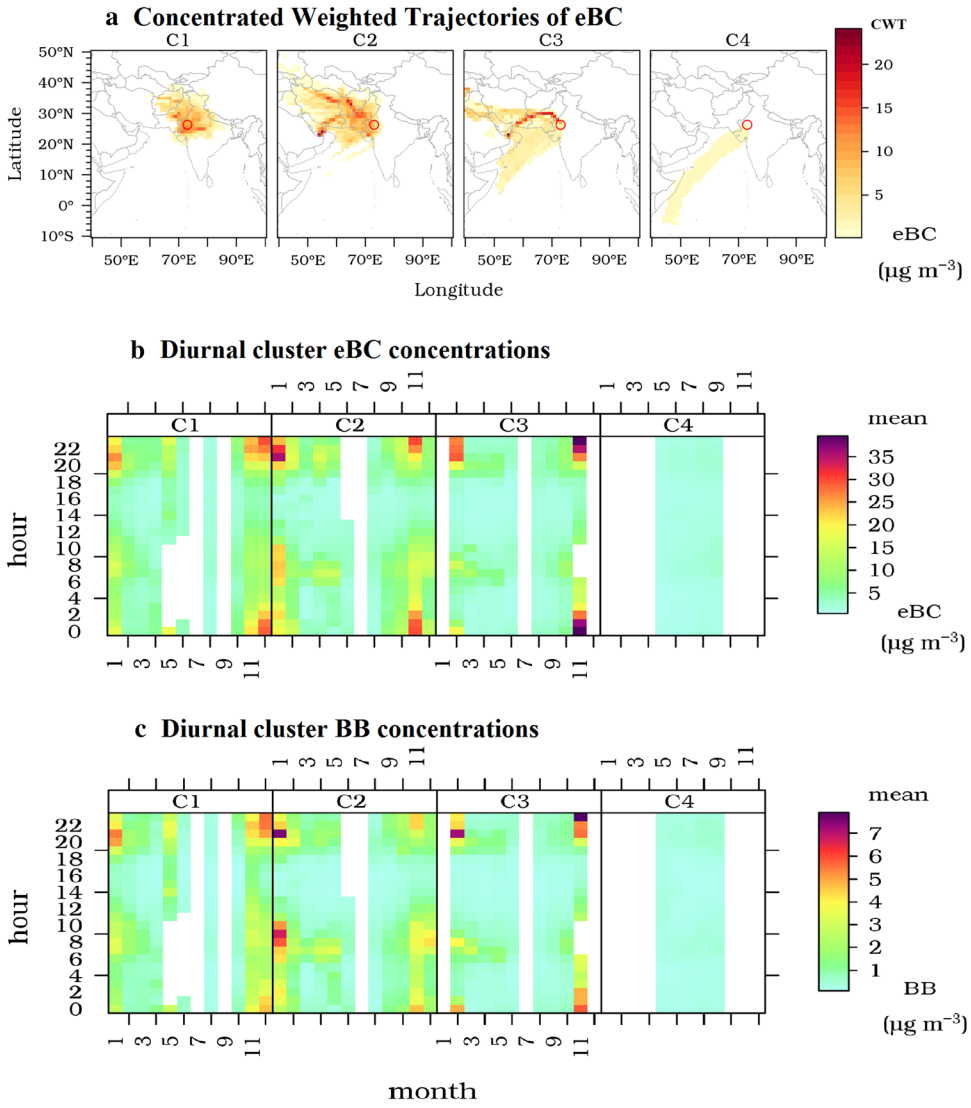

Fig. 10 **a** Concentrated weighted trajectories of Cluster groups C1, C2, C3 and C4 at Jodhpur, 2016. **b** Monthly CWT Diurnal eBC means of four groups of clusters and **c** monthly CWT Diurnal BB means of four groups of clusters during the study period

Table 2 Cluster means of eBC, BB concentrations in μg m^{-3}

Cluster name	% of all trajectories	Mean eBC concentrations of all trajectories (μg m^{-3})	Mean BB concentrations of all trajectories (μg m^{-3})
C1	40.8%	3351	671
C2	26.8%	3373	604
C3	17.5%	2442	478
C4	14.9%	1227	207

Figure 10b, c shows the monthly mean of diurnal variation of EBC and BB concentration which belong to a particular group of cluster. The highest mean concentration of EBC and BB is found in C3 cluster whose group mean path is South West of the observational site in November (Fig. 10c). The C1 cluster carries more amount of BB concentration from the surrounding side of the observational site.

5 Conclusions

A comprehensive analysis was carried out on diurnal and seasonal variations and source identification of Equivalent Black Carbon (EBC) and Biomass Burning aerosol (BB) at Jodhpur using one year data of 2016. The annual mean EBC and BB concentrations are 5.76 and 1.07 μg m^{-3}, respectively. Monthly mean BC concentration is minimum in July 1.41 μg m^{-3} and maximum value of 12.12 μg m^{-3} in January. Further, at seasonal scale, the highest concentration is observed in winter (10.28 μg m^{-3}) and the lowest in summer season (1.71 μg m^{-3}).

Stable meteorological conditions and regional transport from the surrounding areas are the major contributor for the increase of EBC concentrations. The higher BB concentrations clearly indicate the influence of crop residue burning. The higher compensation parameter, which is an indicator of fresh aerosols, is found during crop residue burning periods. Aged aerosols with lower K are associated with greater wind speeds and longer back trajectory pathways from south and south west direction.

The CWT analysis confirms that the most potential source region influencing the receptor site Jodhpur during winter is North-west and North-east region comprising Punjab, Haryana and adjoining Pakistan. A highest 40.8% of trajectories belong to the C1 group of cluster. Monthly mean diurnal cluster means are higher in mid night hours but not during the peak traffic hours. This indicates that the long-range transport is the major source in Jodhpur.

Very low EBC and BB concentrations were reported at the measurement site when the trajectories belong to the C4 cluster originating in monsoon months.

Acknowledgment Authors are thankful to NOAA for providing offline HYSPLIT trajectory model used in this study. The authors are also thankful to Director General of Meteorology and Head of NCMRWF for encouragement to carry out this work. The authors are also thankful to the unknown reviewers for their valuable suggestions.

References

Ashbaugh LL, Malm WC, Sadeh WZ (1985) A residence time probability analysis of sulfur concentrations at grand Canyon National Park. Atmos Environ 19:1263–1270

Babu SS, Manoj MR, Moorthy KK et al (2013) Trends in aerosol optical depth over Indian region: potential causes and impact indicators. J Geophys Res Atmos 118:11794–11806

Bäumer D, Vogel B, Versick S, Rinke R, Möhler O, Schnaiter M (2008) Relationship of visibility, aerosol optical thickness and aerosol size distribution in an ageing air mass over South-West Germany. Atmos Environ 42:989–998

Bond TC, Habib G, Bergstrom RW (2006) Limitations in the enhancement of visible light absorption due to mixing state. J Geophys Res 111:D20211

Bond TC et al (2013) Bounding the role of black carbon in the climate system: a scientific assessment. J Geophys Res Atmos 118:5380–5552

Carslaw D (2015) The openair manual open-source tools for analysing air pollution data. King's College, London, p 287

Carslaw DC, Beevers SD (2013) Characterising and understanding emission sources using bivariate polar plots and k-means clustering. Environ Model Softw 40:325–329

Carslaw DC, Ropkins K (2012) openair - an R package for air quality data analysis. Environ Model Softw 27–28:52–61

Chan L, Deng QH, Liu WW, Huang BL, Shi LZ (2012) Characteristics of ventilation coefficient and its impact on urban air pollution. J Cent South Univ Technol 19:615–622

D'Almeida GA (1986) A model for Saharan dust transport. J Clim Appl Meteorol 25:903–916

Draxler RR (1998) An Overview of the HYSPLIT_4 Modelling System for Trajectories, Dispersion, and Deposition. Aust Meteorol Mag 47:295–308

Drinovec L, Močnik G, Ježek I, Petit JE, Sciare J, Favez O, Zotter P, Wolf R, Prévôt ASH, Hansen ADA (2013) Indication of aerosol aging by Aethalometer optical absorption measurements 32. In: AAAR annual conference, Sep 2013, Portland, United States

Drinovec L, Močni G, Zotter P, Prévôt ASH, Ruckstuhl C, Coz E, Rupakheti M, Sciare J, Müller T, Wiedensohler A, Hansen ADA (2015) The "dual-spot" Aethalometer: an improved measurement of aerosol black carbon with real-time loading compensation. Atmos Meas Tech 8:1965–1979

Drinovec L, Gregoric A, Zotter P et al (2017) The filter-loading effect by ambient aerosols in filter absorption photometers depends on the coating of the sampled particles. Atmos Meas Tech 10:1043–1059
Eck TF, Holben BN, Sinyuk A, Pinker T, Goloub P, Chen H, Chatenet B, Li Z, Singh RP, Tripathi SN, Reid JS, Giles DM, Dubovik O, O'Neill NT, Smirnov A, Wang P, Xia X (2010) Climatological aspects of the optical properties of fine/coarse mode aerosol mixtures. J Geophys Res 115(D19):1–20
Engelstaedter S, Tegen I, Washington R (2006) North African dust emissions and transport. Earth Sci Rev 79(1–2):77–100
Ensor DS, Porch WM, Pilat MJ, Charlson RJ (1971) Influence of the atmospheric Aerosol on Albedo. J Appl Meteorol 10:1303–1306
Fleming ZL, Monks PS, Manning AJ (2012) Review: untangling the influence of air-mass history in interpreting observed atmospheric composition. Atmos Res 104–105:1–39
Ghiaus C, Allard F, Santamouris M, Georgakis C, Nicol F (2006) Urban environment influence on natural ventilation potential. Build Environ 41:395–406
Goudie AS, Middleton NJ (2001) Saharan dust storms: nature and consequences. Earth Sci Rev. https://doi.org/10.1016/S0012-8252(01)00067-8
Grange SK, Lewis AC, Carslaw DC (2016) Source apportionment advances using polar plots of bivariate correlation and regression statistics. Atmos Environ 145:128–134
Haywood JM, Ramaswamy V (1998) Global sensitivity studies of the direct radiative forcing due to anthropogenic sulfate and black carbon aerosols. J Geophys Res Atmos 103:6043–6058
Healy RM, Sofowote U, Su Y, Debosz J, Noble M, Jeong CH, Wang JM, Hilker N, Evans GJ, Doerksen G, Jones K, Munoz A (2017) Ambient measurements and source apportionment of fossil fuel and biomass burning black carbon in Ontario. Atmos Environ 161:34–47
Henriksson SV, Pietikäinen JP, Hyvärinen AP, Räisänen R, Kupiainen K, Tonttila J, Hooda R, Lihavainen H, O'Donnell D, Backman L, Klimont Z, Laaksonen A (2014) Spatial distributions and seasonal cycles of aerosol climate effects in India seen in a global climate–aerosol model. Atmos Chem Phys 14:10177–10192
Henry RC, Chang YS, Spiegelman CH (2002) Locating nearby sources of air pollution by nonparametric regression of atmospheric concentrations on wind direction. Atmos Environ 36(13):2237–2244
Kaufman YJ, Koren I (2006) Smoke and pollution aerosol effect on cloud cover. Science 313:655–658
Kirchstetter TW, Novakov T, Hobbs PV (2004) Evidence that the spectral dependence of light absorption by aerosols is affected by organic carbon. J Geophys Res D Atmos 109(D21):1–12
Lack DA, Cappa CD (2010) Impact of brown and clear carbon on light absorption enhancement, single scatter albedo and absorption wavelength dependence of black carbon. Atmos ChemPhys 10:4207–4220
Moosmüller H, Chakrabarty RK, Arnott WP (2009) Aerosol light absorption and its measurement: a review. J Quant Spectrosc Radiat Transf. 110:844–878
Moosmüller H, Chakrabarty RK, Ehlers KM, Arnott WP (2011) Absorption Ångström coefficient, brown carbon, and aerosols: basic concepts, bulk matter, and spherical particles. Atmos Chem Phys 11:1217–1225
Otto S, Bierwirth E, Weinzierl B, Kandler K, Esselborn M, Tesche M, Schladitz A, Wendisch M, Trautmann T (2009) Solar radiative effects of a Saharan dust plume observed during SAMUM assuming spheroidal model particles. Tellus B: Chem Phys Meteorol 61(1):270–296
Petzold A, Ogren JA, Fiebig M et al (2013) Recommendations for the interpretation of "black carbon" measurements. Atmos Chem Phys Discuss 13:9485–9517
Prasad VS, Johny CJ, Mali P, Singh SK, Rajagopal EN (2017) Global retrospective analysis using NGFS for the period 2000–2011. Curr Sci 112(2):370–377
Prather KA, Hatch CD, Grassian VH (2008) Analysis of atmospheric aerosols. Annu Rev Anal Chem 1:485–514
Prospero JM, Ginoux P, Torres O et al (2002) Environmental characterization of global sources of atmospheric soil dust identified with the Nimbus 7 Total Ozone Mapping Spectrometer (TOMS) absorbing aerosol product. Rev Geophys 40(1):2.1–2.31
Ramanathan V, Li F, Ramana MV et al (2007) Atmospheric brown clouds: hemispherical and regional variations in long-range transport, absorption, and radiative forcing. J Geophys Res Atmos 112:1–26
Russell PB, Bergstrom RW, Shinozuka Y, Clarke AD, DeCarlo PF, Jimenez JL, Livingston JM, Redemann J, Dubovik O, Strawa A (2010) Absorption Angstrom Exponent in AERONET and related data as an indicator of aerosol composition. Atmos Chem Phys 10(3):1155–1169
Sandradewi J, Prévôt SH, Alfarra MR, Szidat S, Wehrli MN, Ruff M, Weimer S, Lanz VA, Weingartner E, Perron N, Caseiro A, Kasper-Giebl A, Puxbaum H, Wacker L, Baltensperger U (2008a) Comparison of several wood smoke markers and source apportionment methods for wood burning particulate mass. Atmos Chem Phys Discuss 8:8091–8118
Sandradewi J, Prévôt ASH, Weingartner E et al (2008b) A study of wood burning and traffic aerosols in an Alpine valley using a multi-wavelength Aethalometer. Atmos Environ 42:101–112
Sateesh M, Soni VK, Raju PVS (2018) Effect of Diwali firecrackers on air quality and aerosol optical properties over a mega city (Delhi) in India. Earth Syst Environ 2(2):293–304
Singh A, Dey S (2012) Influence of aerosol composition on visibility in megacity Delhi. Atmos Environ 62:367–373
Singhvi AK, Kar A (2004) The aeolian sedimentation record of the Thar desert. Proc Indian Acad Sci Earth Planet Sci 113(3):371–401
Sirois A, Bottenheim JW (1995) Use of backward trajectories to interpret the 5-year record of PAN and O"SUB 3" ambient air concentrations at Kejimkujik National Park, Nova Scotia. J Geophys Res 100(D2):2867–2881
Sokolik IN, Toon OB (1996) Direct radiative forcing by anthropogenic airborne mineral aerosols. Nature 381:681–683
Soni VK, Pandithurai G, Pai DS (2016) Is there a transition of solar radiation from dimming to brightening over India? Atmos Res 169:209–224
Stein AF, Draxler RR, Rolph GD, Stunder BJB, Cohen MD, Ngan F (2015) NOAA's hysplit atmospheric transport and dispersion modeling system. Bull Am Meteorol Soc 96:2059–2077
Stier P, Seinfeld JH, Kinne S, Boucher O (2007) Aerosol absorption and radiative forcing. Atmos Chem Phys Discuss 7:7171–7233
Stohl A (1996) Trajectory statistics-A new method to establish source-receptor relationships of air pollutants and its application to the transport of particulate sulfate in Europe. Atmos Environ 30:579–587
Stohl A (1998) Computation, accuracy and applications of trajectories—a review and bibliography. Atmos Environ 32(6):945–1140
Tegen I, Hollrig P, Chin M, Fung I, Jacob D, Penner J (1997) Contribution of different aerosol species to the global aerosol extinction optical thickness: estimates from model results. J Geophys Res Atmos 102(D20):23895–23915
Virkkula A, Chi X, Ding A, Shen Y, Nie W, Qi X, Zheng L, Huang X, Xie Y, Wang J, Petäjä T, Kulmala M (2015) On the interpretation of the loading correction of the aethalometer. Atmos Meas Tech 8:4415–4427
Yu H (2002) Radiative effects of aerosols on the evolution of the atmospheric boundary layer. J Geophys Res 107:4142–4146
Zotter P, Herich H, Gysel M, El-Haddad I, Zhang Y, Močnik G, Hüglin C, Baltensperger U, Szidat S, Prévôt ASH (2017) Evaluation of the absorption Ångström exponents for traffic and wood burning in the Aethalometer-based source apportionment using radiocarbon measurements of ambient aerosol. Atmos Chem Phys 17:4229–4249